


ORIGINAL INNOVATION

Open Access



Failure investigation of a propped cantilever truss bridge

Rabindra Adhikari¹, Lalit Bhatt², Rewati Baruwal², Dipendra Gautam^{3*}  and Rajesh Rupakhety³

*Correspondence:
dig17@hi.is

¹ Department of Civil Engineering, Cosmos College of Management and Technology, Lalitpur, Nepal

² Interdisciplinary Research Institute for Sustainability, Kathmandu, Nepal

³ Earthquake Engineering Research Center, Faculty of Civil and Environmental Engineering, University of Iceland, Selfoss, Iceland

Abstract

Propped cantilever truss is not a common bridge construction technique. The performance of such bridges under operational and extreme loading is not reported in the literature either. In this paper, failure mechanisms in a propped cantilever truss bridge are reported using field investigation. The field observations are supplemented by numerical analysis to identify the causes of failure. A systematic account of damage mechanisms in bridge components is also reported. The failure of the Lamgadi Bridge over the Seti River in Nepal is used as a case study example. The loading and construction protocols are detailed, and numerical analysis results are juxtaposed with the field observations to explain the failure mechanisms. Field observations and numerical results show that lack in adequate design is the most likely cause of the bridge collapse. Numerical results also indicate that the roller support at the propped end, unlike the hinged pot bearing used in the as constructed bridge would have been a safer choice. The failure could have been easily prevented with proper numerical simulation of the bridge response during the design phase.

Keywords: Propped cantilever, Truss bridge, Bridge collapse, Failure mechanism, Forensic analysis, Loading protocol

1 Introduction

Due to dynamic actions and other causes such as construction deficiencies, bridge damage/collapse can occur during construction or operation. Bridge failure results in huge economic consequences (Gautam and Rupakhety 2021) together with operational losses, traffic disruption, and extended travel time. Bridge failure due to dynamic actions is well accounted for in the existing literature (see e. g. Shinozuka et al. 2002; Gautam, Rupakhety, and Adhikari 2019; Adhikari et al. 2019; Gautam 2017; Gautam et al. 2023). Similarly, collapse cases without dynamic actions are also reported as case studies (see e. g. Cao, El-Tawil, and Agrawal 2020; Brando et al. 2013; Salem and Helmy 2014; Anania, Badalà, and D'Agata 2018; Adhikari et al. 2022). Sun, Sun, and Li (2007) presented damage mechanisms of a curved continuous bridge arising from an unstable displacement after two years of operation. Calvi et al. (2019) and Calvi et al. (2021) concluded that the failure of the Morandi bridge in Italy was attributed to either deck or antenna stay connection failure. They numerically justified that removal of one of the bridge stays would define the collapse mechanism in terms of flexural-torsional-shear demand.

More detailed explanations and failure investigation of the same bridge were subsequently reported by Scattarreggia et al. (2022). Scattarreggia et al. (2022a, b) numerically assessed the collapse of Capriogliola bridge in Italy using applied element modeling (AEM). Synthesizing forensic evidence with numerical modeling, they concluded that the movement of one of the bridge piers or abutments was the most likely cause of the failure. Bazzucchi, Restuccia, and Ferro (2018) identified the failure causes as the lack of adequate ductility, periodic maintenance, durability issues, and monitoring problems, among others. Schaap and Caner (2022) concluded that the major causes of failure in Turkish bridges are hydraulic event and vehicle collisions, respectively for highway and pedestrian bridges. Similar case studies and forensic damage/failure analyses are also reported elsewhere (see e. g. Nuti et al. 2020; Vatansever et al. 2020; Sakellariadis, Anastasopoulos, and Gazetas 2020).

Although failure/damage mechanisms in reinforced concrete (RC), steel, precast RC bridges are frequently reported, similar studies covering propped cantilever truss bridges are rare, if not absent, in the literature. We present a detailed account of failure mechanisms in a propped cantilever truss bridge considering the failure case study of the Lamgadi Bridge over the Seti River in Nepal. Field investigation and numerical modeling are assimilated to define the governing causes of the failure. Insights into propped cantilever truss bridge collapse and potential mitigation measures are also outlined.

2 Materials and methods

2.1 Lamgadi propped cantilever truss bridge

On January 24, 2022, the bridge connecting Gagangauda (Pokhara Metropolitan City ward 32) and Lamgadi (Pokhara Metropolitan City ward 33) over the Seti River in western Nepal collapsed before opening for the regular traffic. The bridge is a propped cantilever steel truss bridge with reinforced concrete deck. This is the first bridge of its type in Nepal. The bridge has a total span of 60 m with three trusses supporting a continuous concrete deck slab. The bridge was initially designed with 7.5 m carriageway width and 1.25 m sidewalk width on each side. The total width was later reduced to 7.2 m with 6 m wide carriageway 0.6 m sidewalk on each side. Each side of the deck has 1 m tall GI (Galvanized Iron) pipe railing. The deck slab is 200 mm at the edge and 275 mm at the center with 2.5% camber. The sidewalk is 300 mm above the carriageway. Joints in concrete deck are provided only between the abutments and the deck. The general arrangements of the structural system and the major components of the bridge are presented in Fig. 1. Similarly, Fig. 2 shows the structural system, bearings, and formworks. RC deck slab was cast in-situ over the top cross beam which is anchored to five shear connectors (SC) per beam, while the top cross beam is connected to the top-chord of the truss with six steel cleat angles (CA) per beam as detailed in Fig. 3. M-20 RC slab is used as the deck.

Most of the members are built-up sections with steel plate lacings at regular intervals. All steel components are made of Fe-410 grade steel. The total weight of steel elements is estimated to be around 160 tons including nuts and bolts but excluding the weight of galvanization and deduction for holes and other machining losses. The bridge was designed to have fixed support at one end and roller support on the other end. The fixed end is supported on bearings A1 and A2, while the propped end is supported on bearing

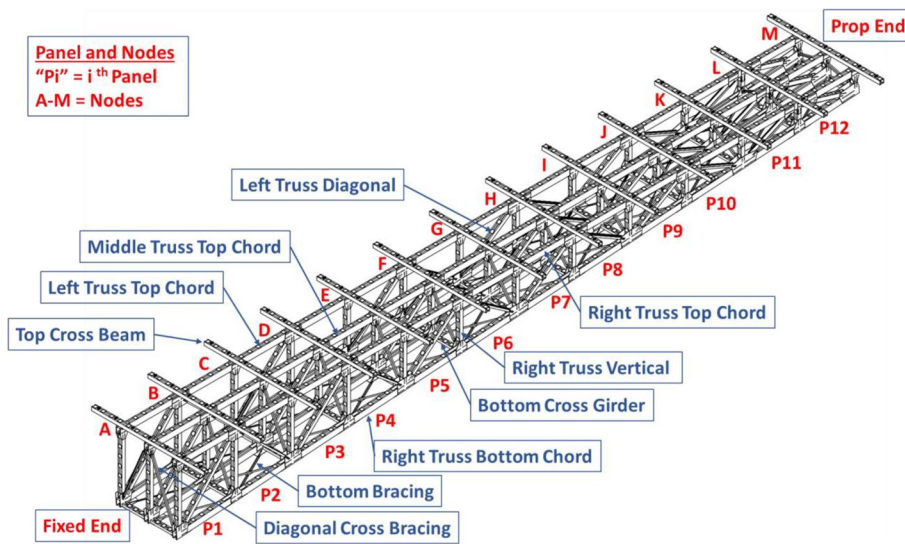


Fig. 1 General arrangement of steel structure of the bridge

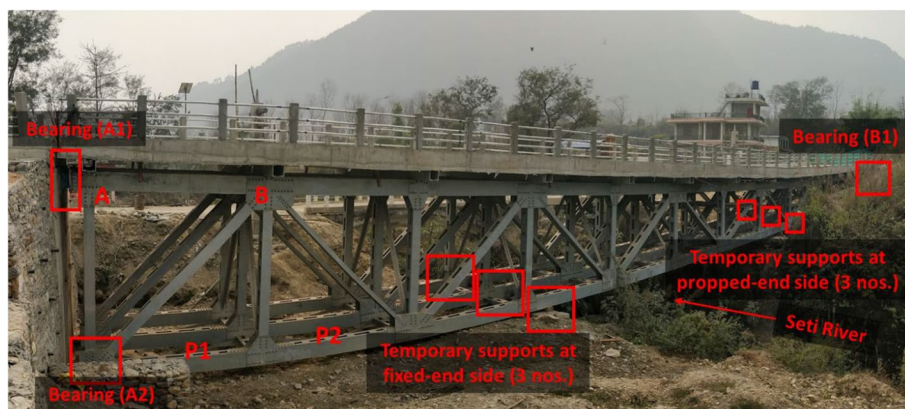


Fig. 2 Arrangements of bridge structure, bearings, and temporary supports

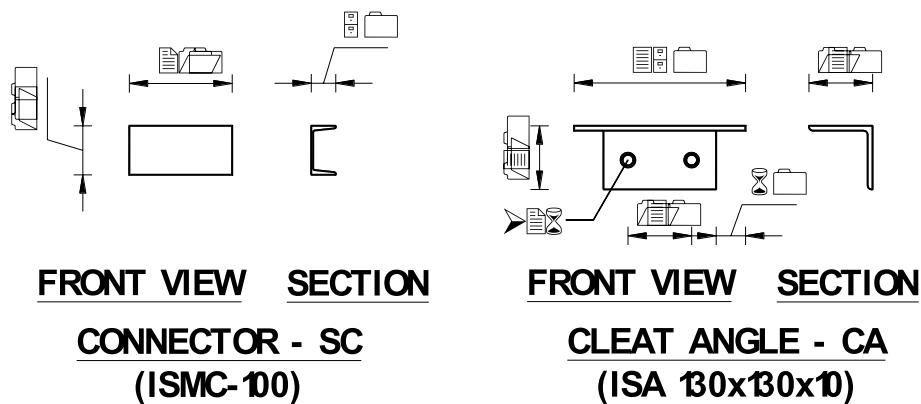


Fig. 3 Detail of shear connector (SC) and cleat angle (CA). All dimensions are in mm

B1. Details of the bearings are shown in Fig. 4. Three sets of bearings are provided at each location for three steel trusses.

2.2 Field investigation and forensic analysis

Field observation of the collapsed bridge was carried out on February 1-2, 2022. Detailed assessment of each component was conducted, and failure mechanisms were documented. Relevant measurements were taken at each damage location. Several local people and authorities were interviewed to investigate if pre-failure signs and other anomalies were detected prior to the collapse. The observed damage mechanisms and numerical modeling are presented in detail in the following sections.

3 Results and discussions

3.1 Failure mechanisms

Failure of several components was observed during the field investigation campaign. The bridge deck settled significantly with the maximum settlement of 801 mm at joint I as shown in Fig. 5. Some top chords, top cross beams, and bearings were found to be damaged as well. There was no visible damage such as buckling or tearing on the bottom chord members. While no damage was observed on the vertical elements, diagonal elements, horizontal bracings, and vertical bracings, several connections were found to be damaged. The details of damage to each component are presented in the following section.

3.1.1 Damage to top cross beams

Rotation of the cross beams supporting the deck near the propped end was observed as shown in Fig. 6a. At joint M (see Fig. 2), which is the propped end, rotation of the cross beam resulted in the displacement of 68 mm between its top and bottom faces. Meanwhile, the beam did not slide relative to the deck. As shown in Fig. 5, the rotation of the bridge axis is the largest at joint M, which explains a significant rotation of the cross beam at this joint. At joint L, where the rotation of the bridge axis is the lowest, the cross beam slid by ~86 mm relative to the slab, while its rotation was not significant. Sliding between the deck slab and cross beams was observed only at two other cross beams: about 77 mm at joints J and K. Sliding between the top beams and the deck slab occurred only on the side of the bridge toward the propped end from the point where the deck deflection is maximum.

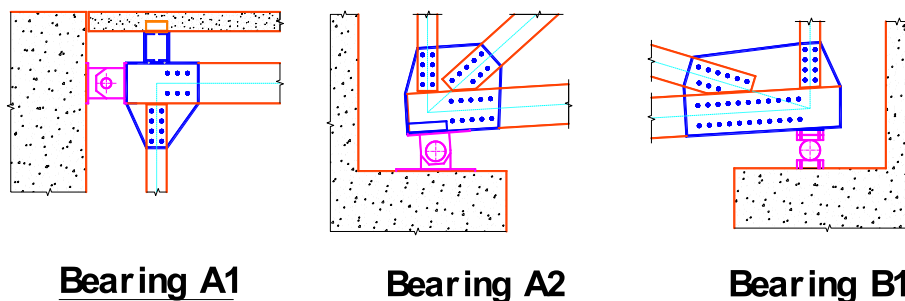


Fig. 4 Schematic representation of the bearings (refer Fig. 2 for the location)

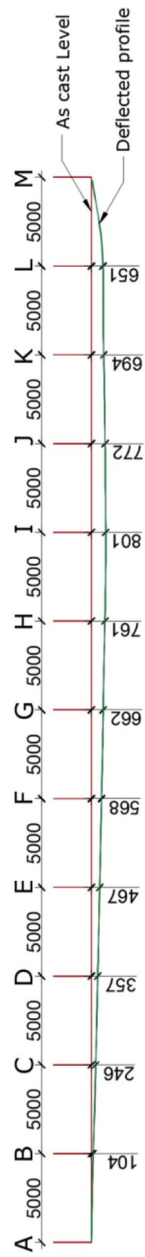


Fig. 5 Settlement profile of the bridge along the length. All dimensions are in mm.



Fig. 6 Observed damage in top cross beam: **a** joint M, **b** joint L, **c** joint K, **d** joint J, **e** joint I at right truss, **f** joint I at left truss, and **g** joint H

3.1.2 Damage to cleat angles

Cleat angles (see Fig. 3) were used to connect the top chord of the truss with top cross beams. Deflection of the bridge resulted in rotation of the top chord members, which caused the flange of the cleat angles connected to the top beams to bend. This resulted in tearing of the flange on one side. Then tearing of the cleat angles caused the top beams to rotate. Tearing was maximum at the propped end where the rotation of the deflected bridge is maximum. As shown in Fig. 7, damage was mostly concentrated at the propped end, which reduced gradually toward the center of the span. At joint L, the top beam slid

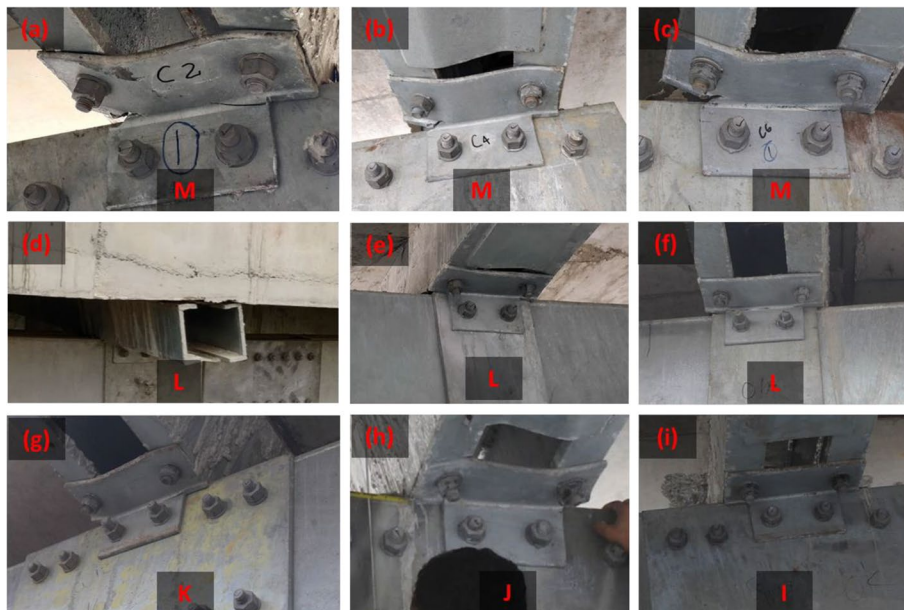


Fig. 7 Damage to cleat angles (uppercase alphabets in the figure represent the node IDs of the grid in which the joints are located)

relative to the deck meanwhile the cleat angle did not bend, this explains the lack of rotation of the top beam at this joint.

3.1.3 Damage to bearings

Some of the bearings were found to be damaged. Bearing A1 is steel hinge bearing at the top of the fixed end, bearing A2 is hinge roller type pot bearing at the bottom of the fixed end side, and bearing B1 is hinge type pot bearing at the propped end. A schematic diagram of the pot bearing is presented Fig. 8. Figure. 9 shows the arrangement of hinge type pot bearing (bearing B1). An additional wedge plate was used to accommodate the designed slope of the bottom chord of the truss. The wedge plate was welded over the sole plate of the bearing. The bottom plate connected to the bottom face of the bottom chord of the truss was also welded. The truss bottom plate was connected to the truss element with bolted connection outside the bearing but welded over the bearing as bolted connection was not possible in this part as shown in Fig. 10. Significant rotation of bearing was observed at bearing B1 with some torsion on one of the bearings while some sliding was observed at bearing A2.

As shown in Fig. 11, all three bearings of B1 underwent significant rotation of about 8° due to deflection of truss. While no sliding was observed in any of the bearings B1, there was connection damage (weld damage) between the bottom chord of the truss and the wedge plate over the sole (top) plate of the bearing. Under the right truss there was about 11° of torsion of the bearing plate, but no noticeable torsion was observed at the other bearings.

The arrangement of hinge roller type pot bearing at bearing A2 is shown in Fig. 12. The connection details are similar to that of the bearing B1; however, bearing A2 allows relative displacement of top bearing plate against the pot in the longitudinal direction. As shown in Fig. 13, the top plate, and the truss as well, moved toward the abutment with a sliding mechanism between the guide plate and the guide of the bearing. Also, not significant though, there was noticeable rotation at the pot bearing. The arrangement of steel hinge bearing at A1 is shown in Fig. 14, which did not observe any damage.

3.1.4 Damage to the top chord

Three top chord members were found to be significantly damaged. The left top chord of panel-8 (L:TCH-8), middle top chord of panel-9 (M:TCH-9), and right top chord of panel-9 (R:TCH-9) were found to be buckled. The middle top chord of panel-8 (M:TCH-8) and middle top chord of panel-10 were also found to have slight local buckling as shown in Fig. 15.

L:TCH-8 sustained localized damage near the connection as shown in Fig. 16. There was a local instability of the flange and web, most likely due to excessive compression. However, no tearing or damage to bolting or welding near the damage location was observed.

In the middle truss, M:TCH-9 was buckled excessively toward the downstream side by about 180 mm at a distance of 1550 mm from joint I. There was a local instability at M:TCH-8 near joint I, excessive buckling of M:TCH-9, and then again slight local buckling of M:TCH-10 near joints J and K as shown in Fig. 17.

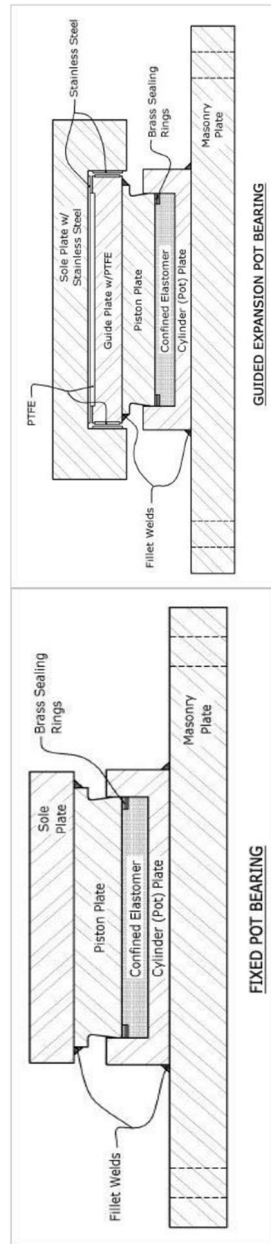


Fig. 8 Schematic diagrams of hinge-type (left) and roller-type (right) bearings

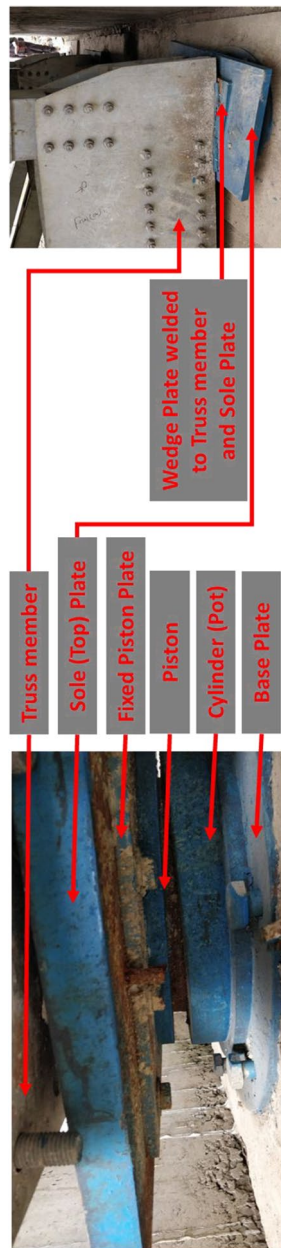


Fig. 9 Site arrangement of bearing B1

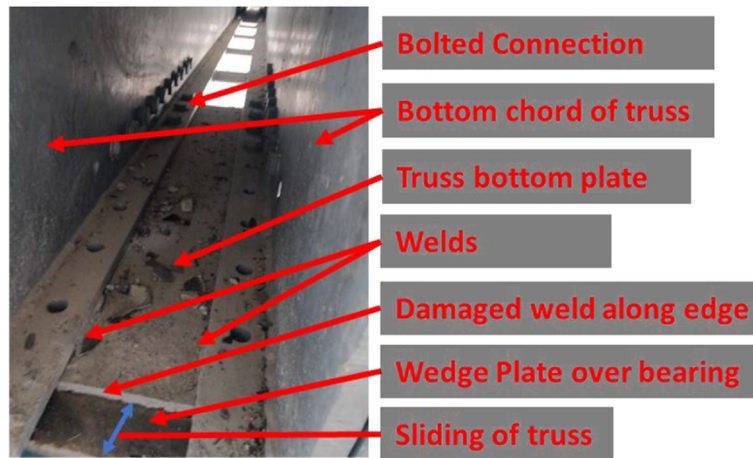


Fig. 10 Connection of truss and bearing at bearing B1



Fig. 11 Damage to bearing B1: **a** bearing under the left truss with significant rotation, **b** bearing under the middle truss with significant rotation, **c** bearing under the right truss with significant rotation as well as torsion about vertical axis

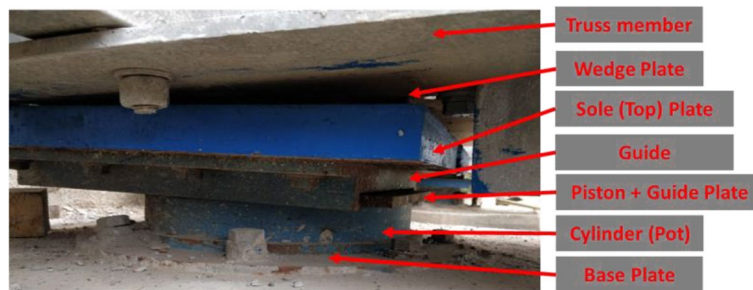


Fig. 12 Arrangement of bearings A2 depicting displacement of the top plate toward abutment against the pot

In the right truss (upstream side truss) also, a top chord member buckled excessively. R:TCH-9 was excessively buckled on the downstream side with some local buckling near joint I as well (Fig. 18).

3.1.5 Connection damage and misfit

Some of the connections were visibly damaged and certain misfits were also observed. Some of the misfits were corrected in some cases, while left uncorrected in many other

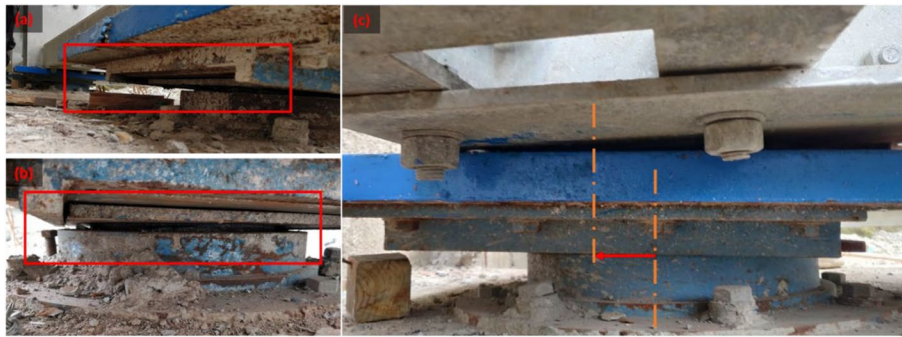


Fig. 13 Sliding at bearings A2: **a** outward movement of the top plate leaving the guide plate inside, **b** noticeable opening between pot and top plate in the abutment side of bearing due to significant rotation, **c** displacement of the top plate toward abutment against the pot



Fig. 14 Steel hinge bearing A1: **a** side view, **b** oblique view, **c** bottom view

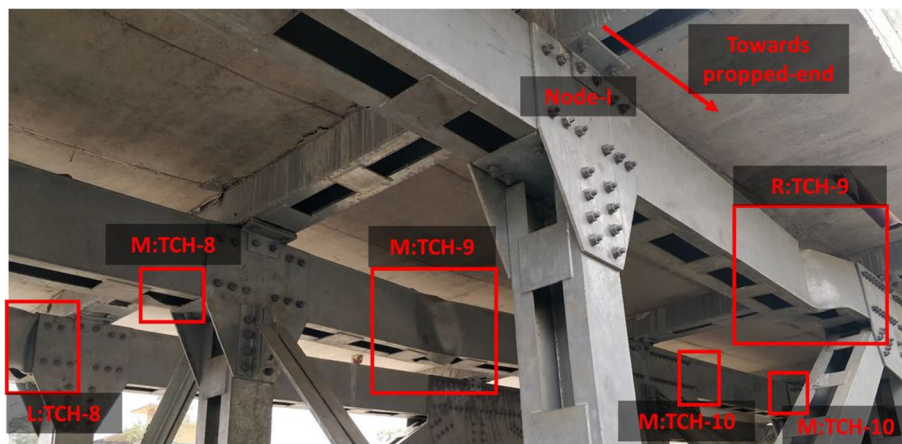


Fig. 15 Observed damage mechanisms in the top chord members

locations. Figure. 19 shows that there was damage to the bolted connection of the vertical connection at node I and some bending of the connecting angle at node H.

A few misfits of members and alignment issues of holes in bolted connections were identified during field investigation. Figure. 20 shows some of the connection issues that include imperfect connection of several vertical braces. Less than three bolts were effective in many vertical brace connections although more bolts were provided.

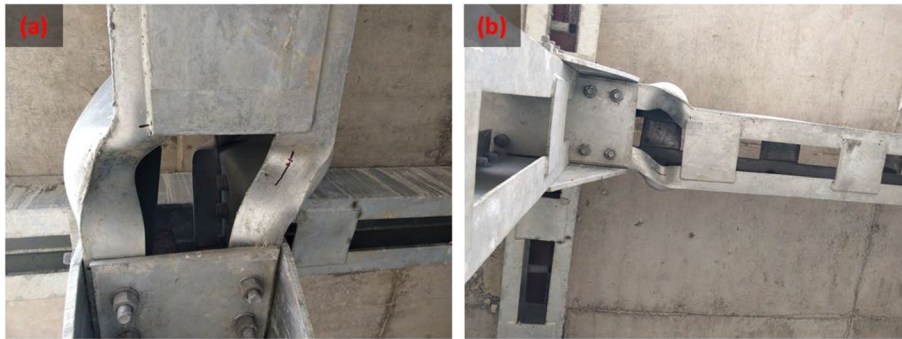


Fig. 16 Damaged top chord of the left truss: **a** close up view from the bottom **b** view from the bottom

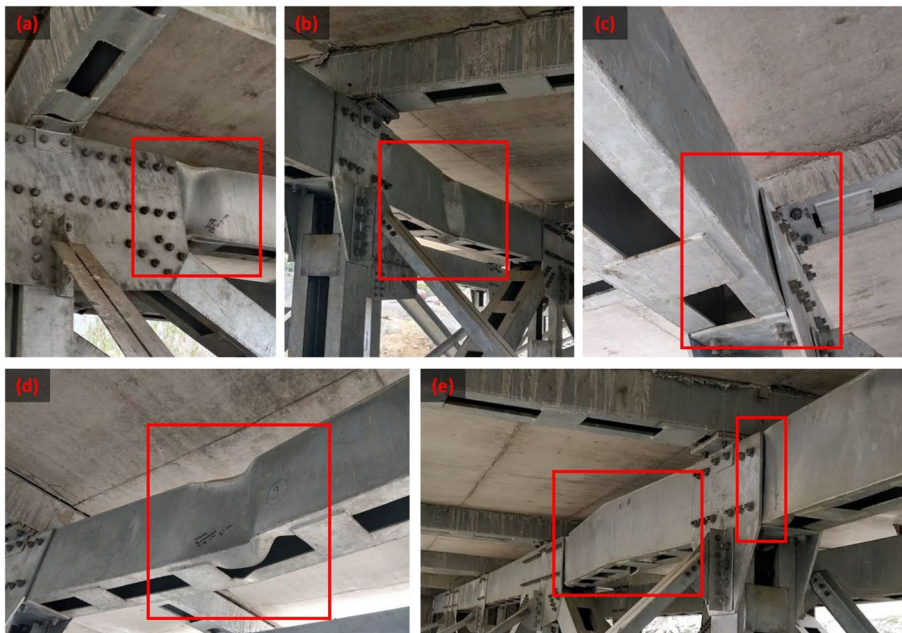


Fig. 17 Observed damage in the top chord of the middle truss: **a** M:TCH-8 damage near joint I, **b** buckled M:TCH-9, **c** local buckling of M:TCH-10 near joint K, **d** interior face of buckled M:TCH-9, **e** exterior face of buckled M:TCH-9 and slight local buckling of M:TCH-10 near joint J

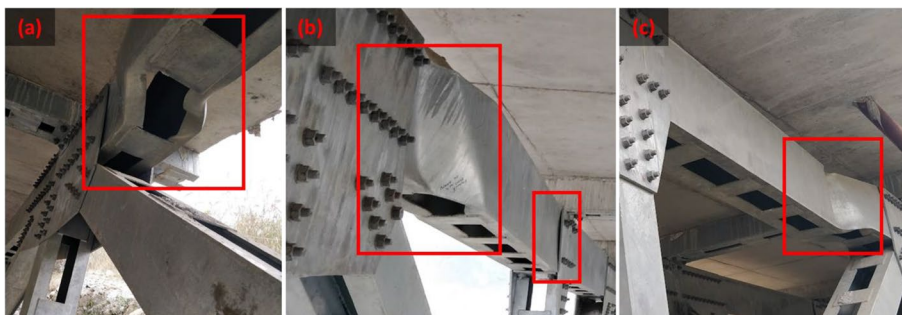


Fig. 18 Damage to the top chord of right truss: **a** bottom view of R:TCH-9, **b** downstream side face of buckled R:TCH-9 and slight local buckling near joint I, **c** upstream side face of buckled R:TCH-9

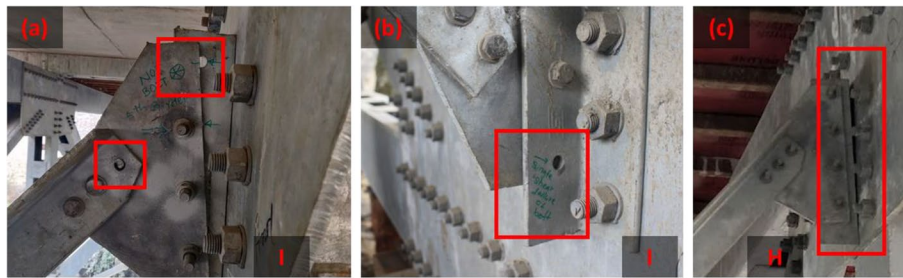


Fig. 19 Connection damage in vertical bracing: **a** at the top connection with middle truss at joint I of the vertical bracing between the middle and right trusses, **b** at the bottom connection with the right truss at joint I of the vertical bracing between middle and right trusses, **c** at the top connection with middle truss at joint H of the vertical bracing between the middle and the right trusses

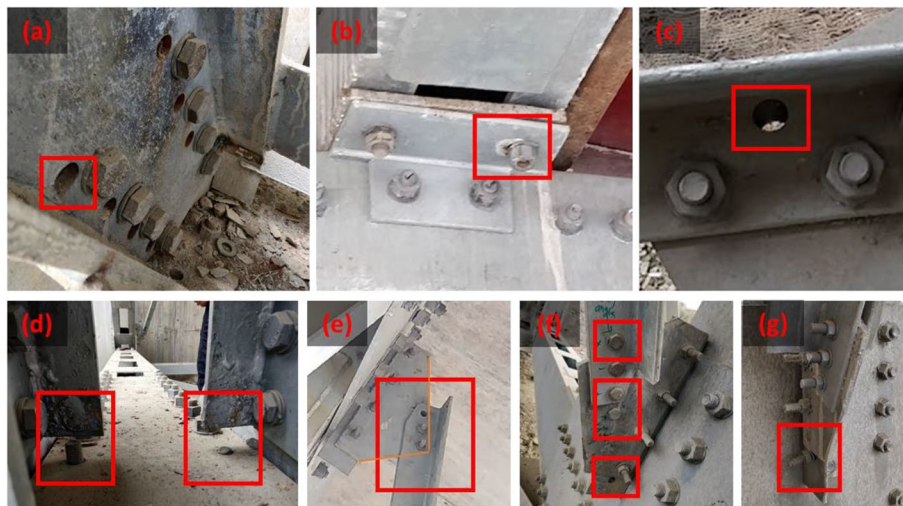


Fig. 20 Construction defects in various parts of the structure: **a** holes drilled twice due to error in the diagonal chord, **b** misalignment of hole in cleat angle, **c** misaligned hole in bottom horizontal bracing, **d** vertical chord prohibiting bolted connection of the top plate of the bottom chord, **e** connection of vertical bracing without sufficient edge distance on gusset plate, **f** less active bolts with two idle bolts and a misaligned hole, **g** inactive bolt on gusset plate

Although it was claimed that all the elements of the bridge were fastened and the builder was ready for load test, some of the bolts were found not well tightened or even missing. A site personnel said that some of the bolts were loosened or removed after the collapse for lifting the bridge; however, we were not able to verify the claim independently. Figure. 21 shows some connections with a few or more bolts in loosened state, which were most likely untouched even after the collapse of the bridge considering the state and location of bolts. Most of the loose bolts of the bottom plate are not directly visible from ground due to obstruction by the diagonal members. Also, a vertical diagonal at joint A was found to be connected slightly eccentrically at the left truss bottom part against the general practice of concentric connection on all other parts and considering the general pattern of construction at site. It was due to the placement of connecting angle in improper orientation, i.e., the outstanding flange of the connection was expected toward the center of the joint, but it was installed toward the abutment.

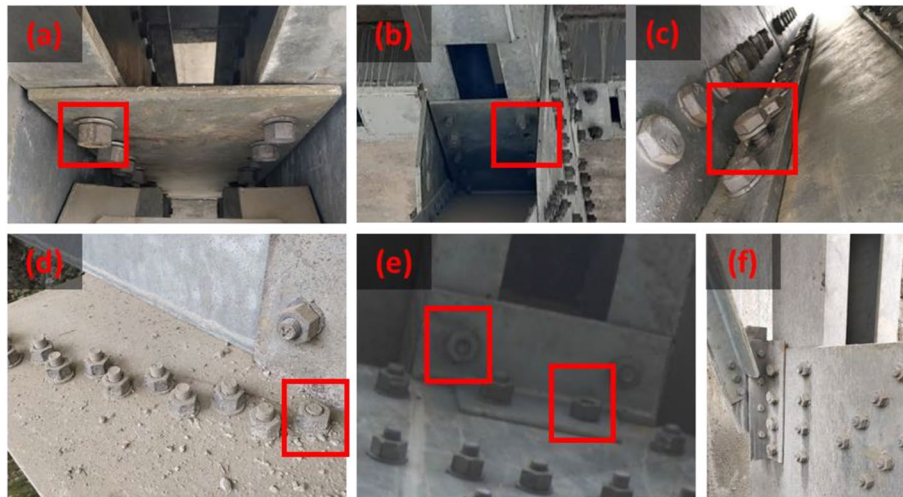


Fig. 21 Connection issues in some parts of the structure: **a** incompletely tightened bolts at the bottom plate of top chord, **b** missing bolts at the bottom plate of the top chord, **c** untightened bolts at the bottom plate of the top chord, **d** untightened bolts at the bottom bracing connection, **e** improperly tightened bolts at the connection of a cleat angle, **f** eccentrically connected vertical bracing

However, this variation is not linked to the cause of the present failure but indicates undesirable workmanship quality of work.

3.2 Numerical modeling

Damage to the bridge initiated during the removal of temporary supports after the completion of fastening work of the steel truss as claimed by the workers involved in casting and hardening of the deck. Three temporary supports at Y (see Fig. 22) were removed without any noticeable damage or deformation. However, during removal of three temporary supports at X by hammering the timber blocks, only a support under the right truss came out and to loosen others they were fired and hammered. During hammering, there was sudden damage after which temporary supports were restored.

We performed scenario analyses using numerical modeling for complete steel truss plus hardened concrete deck without temporary supports, all steel trusses fastened at site without deck slab and temporary supports, complete steel truss plus hardened concrete deck slab with temporary supports at X and Y, complete steel truss plus hardened concrete deck slab with temporary supports at X only, and complete steel truss plus hardened concrete deck slab considering yielding of the temporary supports at X (no support at Y). All the analyses are linear static analyses for self-weight to replicate the field load exposure condition. For each analysis scenario, we adopted as built arrangement of bearings considering when there are roller supports at B1 and hinge supports at A1 (case A) and when hinge supports are provided at B1 and roller supports are provided at A2 (case B). Case B replicates the as constructed condition of the damaged bridge.

We modeled the bridge for all scenarios in finite element program SAP2000 v23.1.0 (Computers and Structures Inc 2018). The truss members were modeled with line (frame) elements. Slab was modeled as a thin shell element. Connections were assumed

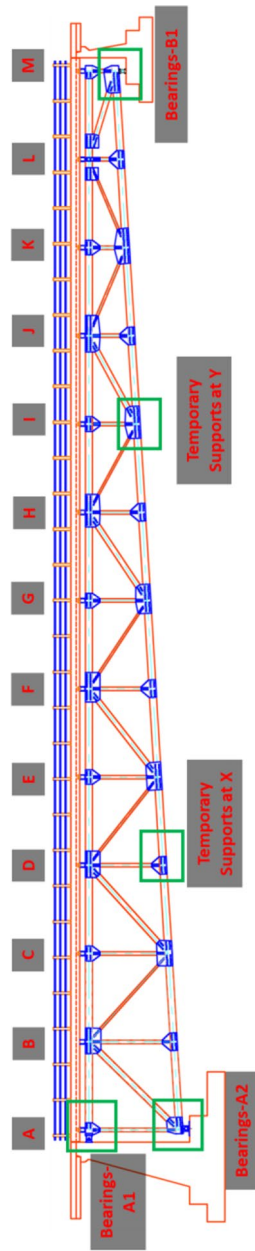


Fig. 22 Arrangement of temporary supports at the end of construction phase

to be rigid, and hinge bearing and roller bearing were assumed to be pure hinge and pure roller in the model. Stiff links were used to connect TCH and TCB and the shear transfer was measured at these links. Sectional representations of some of the elements are presented in Figs. 23 and 24. A three dimensional finite element model of the bridge is shown in Fig. 25.

3.2.1 Scenario I: complete steel truss plus hardened concrete deck without temporary supports

The results of numerical analysis showed that the expected maximum deflection of the bridge under dead load is 43 mm and 79 mm for case A and case B, respectively (Fig. 26).

Similarly, all the estimated member forces were found to be well below their capacities for case A, but a few members were found to be overstressed for case B (Fig. 27). DCH-10 and DCH-12 were especially overstressed with a compression ratio of 1.6 while TCH-9 has compression ratio of almost unity when a design check was done as per the IS 800:2007 guidelines (Bureau of Indian Standard 2007), considering partial safety factors for load and material as unity. For this state, a high compression load needs to be transferred to the deck slab as shown in Fig. 28. It clearly shows that case B requires significantly high compression to be transferred to the deck slab and the slab needs to

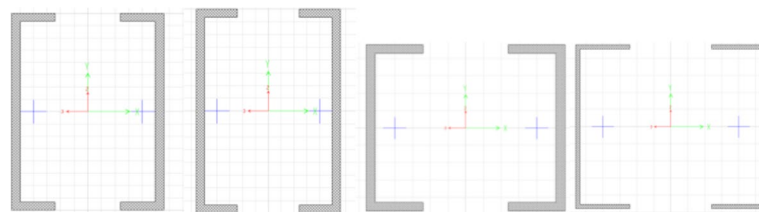


Fig. 23 Typical sections of members TCH, BCH, DCH (built up type), VCH (left to right)

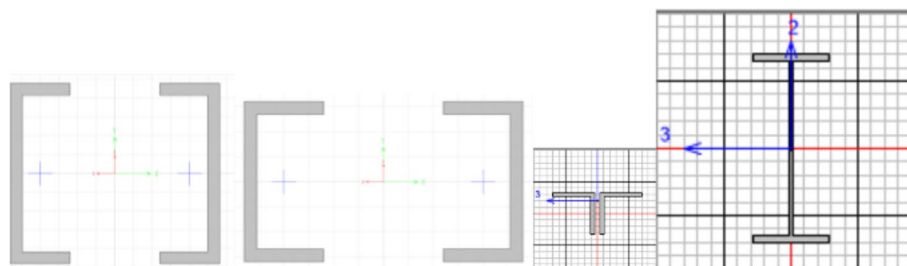


Fig. 24 Typical sections of members TBCH, CGCH, DCB, DCH (rolled section type), (left to right)

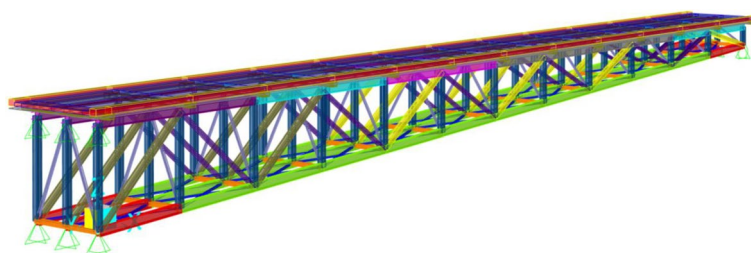


Fig. 25 Three-dimensional finite element model of the bridge



Fig. 26 Deflection of truss for scenario I case A (left) and case B (right)

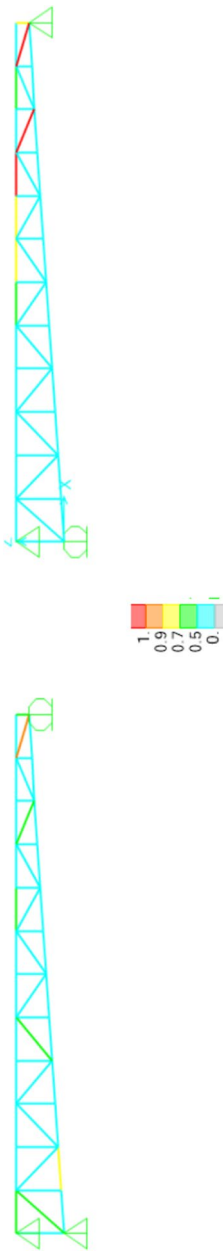


Fig. 27 P-M-M ratio contours for case A (left) and case B (right)

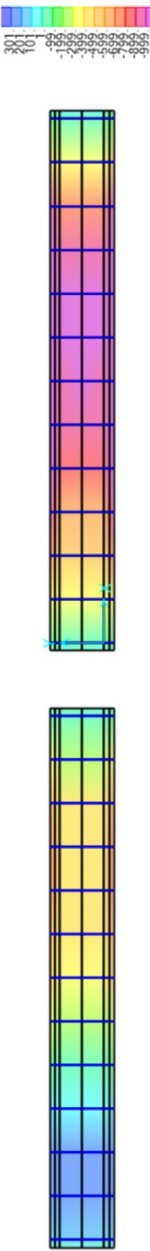


Fig. 28 Compressive force (kN/m) contours on deck slab for case A (left) and case B (right)

resist a compression force of about 1000 KN/m in the longitudinal direction requiring the cross beams at grids M, L, and K to transfer about 1275 KN, 3215 KN, and 1970 KN of shear force from truss top chord to the deck slab for case B against the forces of 897 KN, 1916 KN, and 875 KN, respectively for case A. A simple bending analysis of two 16 mm thick wall of top cross beams for shear deformation shows that the horizontal force of 854 N will start yielding of the wall (web) and has ultimate horizontal resistance of 1400 KN. Shear transfer is significantly large in case B and is the maximum at grid L. The most significant damage was observed at the shear connector of the same grid, which was completely displaced from the original position. Although the calculated forces are high, once yielding starts, these forces will actually reduce due to redistribution of forces due to the deformation and find new equilibrium position unless material stress crosses the ultimate stress. Since all temporary supports were not removed completely, yielding and damage started after a few mm settlement of temporary supports during removal. The analysis also shows that even for case A, a top cross beam at grid L is susceptible of yielding under dead load, though it may not create significant secondary effects.

3.2.2 Scenario II: all the steel truss elements fastened at site without deck slab

At site, after fastening of all truss elements along with bearings, temporary supports were removed to check the connection. Temporary supports were provided at six locations during fastening of steel truss. No anomalies such as damage or excessive deformation can be noticed during the support removal (Fig. 29).

Numerical analysis depicted a deflection of 66 mm for case B at grid I against 28 mm for case A at grid H. As some deflection was expected, but not measured at site, this deviation was not analyzed by the erection team. Also, horizontal inward reaction of 802 KN and the vertical reaction of 684 KN were observed at each bearing B1 for case B against the vertical reaction of 480 KN for case A (Fig. 30).

A design check as per IS 800:2007 considering partial safety factor for load and material as unity was also performed. It showed that the top chords were overstressed in dead load only without deck slab for both cases. The maximum P-M-M ratio (demand to capacity ratio) as defined by IS 800:2007 was found to be 1.8 for TCH-10 (governed by compression) for case A and 2.6 for TCH-9 (governed by compression) for case B. TCH-7 to TCH-10 have the same section with design axial tension capacity and design compression capacity of 2736 KN and 258 KN, respectively for material safety factor of 1. However, no damage was observed at the site. It is because the design strength of compression members is calculated to be much lower due to slenderness effect, but the reduction is not effective at site to the same extent as provisioned by the code, and the members took much higher compression than the compression capacity per the design codes. There could have been initiation of some local buckling of lesser intensity, which was not noticed in the case of short term loading.

3.2.3 Scenario III: complete steel truss plus hardened concrete deck slab with temporary supports at X and Y

Temporary supports were removed for a certain time after fastening. Then, before construction of the deck slab, temporary supports were restored only at two locations X and Y under the truss, which was deflected by about 34.8 mm and 61.2 mm respectively



Fig. 29 Deflection of truss (mm) for case A (left) and case B (right)



Fig. 30 P-M-M ratio contours for case A (left) and case B (right)

as per the numerical analysis results (Fig. 31). Thereafter, RC deck slab was cast, which changed the forces in the system.

Considering the upward reaction by the temporary supports at the site, the vertical deflection of supports at X and Y were set to 34.8 mm and 57 mm (slightly less than 61.2 mm to allow the truss to rest over the temporary supports) in the numerical model to estimate their reactions. The analysis showed that the total reaction on temporary support at Y was just about 100 kN while the total reaction on temporary support at X was about 675 kN. Hence, the worker could easily hammer out the supports at Y, but it was more difficult to remove supports at X as experienced by the site workers.

3.2.4 Scenario IV: complete steel truss plus hardened concrete deck slab with all three temporary supports at X (supports at Y removed)

After the temporary supports at Y were removed, there was an insignificant change in deflection or forces in truss members, because the reactions at Y were relatively small (Fig. 32). Accordingly, workers also did not notice any significant displacement in the members after removal of the temporary supports at Y, which is because the reaction at support Y was relatively small, and it was easily redistributed to the other supports after the removal of temporary supports.

3.2.5 Scenario V: complete steel truss plus hardened concrete deck slab with only two temporary supports at X under the middle and downstream trusses

Stage 1 When the temporary support at X of the downstream side truss was removed, there was some redistribution of the forces in the truss members as shown in Figs. 33, 34, and 35. The numerical results confirm that if the deck slab is not damaged, no significant stress in truss members will be developed even though one of the supports is removed.

Stage 2 During removal of the remaining two temporary supports at X, there was some settlement during burning of the timber block as shown in Fig. 36.

About 10 mm settlement was estimated under the left and middle truss supports at X due to shrinkage of the timber support block. During this loosening process, the horizontal reaction provided by friction was also lost. Hence, the roller at the fixed end and side end started to roll slowly toward the abutment. During this process, the settlement increased significantly, and high compression force was transferred to concrete slab, especially near the propped side. Hence, the connection (cleat angles) started to yield and tear causing tearing sound as heard by the workers. Then, the left top chord underwent local buckling suddenly causing a loud noise.

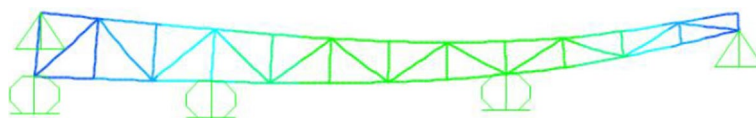


Fig. 31 Provision of temporary supports under steel truss



Fig. 32 Member forces (KN) for scenario III case B (left) and scenario IV case B (right)



Fig. 33 Member forces (KN) for scenario IV and scenario V in the right truss



Fig. 34 Member forces (KN) for scenario IV and scenario V in the middle truss



Fig. 35 Member forces (KN) for scenario IV and scenario V in the left truss



Fig. 36 Temporary supports at X: **a** under the middle and left trusses that were crushed after burning, **b** close up view of temporary support under middle truss, **c** restored temporary support under right truss

Stage 3 As yielding and tearing of cleat angles and shear studs proceeded slowly, the settlement of the truss also increased gradually under self-weight. The top chord of the downstream side truss had already buckled, the force was not balanced, and hence higher compressive forces developed in some of the top chord members of the middle and upstream side trusses. Ultimately, a top chord of each of the middle and upstream side trusses buckled with significant loss of compressive strength and damage to connection with bearings on the propped end sides occurred. During this, major settlement of the deck occurred that resulted in significant damage to the concrete deck as well. The tearing of cleat angles increased considerably and one of the top beams completely detached from the deck. However, after significant sudden settlement due to buckling, the structure settled at a new equilibrium with redistribution of the forces. Slight adjustment continued to occur as the noise continued to be heard by the local people.

4 Conclusions

The purpose of this study is to depict the most likely causes of the failure of a propped cantilever truss bridge. Using the collapse case study of the Lamgadi Bridge over Seti River in Nepal as a case study, failure mechanisms are discussed using field observations and numerical modeling. The damage mechanisms presented in this paper could be insightful for future precaution based design implementation and numerical as well

as experimental assessments. The bridge failed under its self-weight. Excessive deflection of the bridge resulted in buckling of some of the top chord members. As the bridge rotated, cleat angles connecting the top chords to the cross beams bent and tore in tension. This resulted in rotation of the cross beams. Hence, force transfer from the truss to the concrete deck was not effective, as might have been assumed in design. Most of the damage occurred near the propped end of the bridge where the rotation of the bridge axis due to its deflection is the maximum. A propped cantilever structure generally has a roller support at the propped end. The as built structure, however, had a hinged pot bearing at the propped end. Restraint of horizontal motion at the propped end during deflection of the span can generate large compressive forces on the top chord members, as was the case in the Lamgadi Bridge. Apart from this, the bearing at the propped end was not sufficiently strong to transfer the forces caused by the self-weight of the bridge. Numerical analysis of different loading scenarios confirms the field observations to a large extent. The results indicate that buckling of top chord elements is to be expected. Numerical results also show that forces transmitted to the propped end bearing as well as the heavily loaded top chord members are lower when the propped end has a roller support than when it has a hinge support. The choice of hinge support at the propped end in the design of the bridge therefore seems difficult to be justified. Failure of welding at the bearing and several construction defects in the bridge point to the lack of adequate construction supervision. Potential damage during support removal after casting the deck is predicted by the numerical results. The lack of proper numerical modeling during design as well as simulation of load scenarios such as removal of temporary supports proved detrimental to the bridge. Such failures could be easily rectified by proper design and quality control in construction. Although ideally suited for short river crossings across deep gorges, like in the case of the Seti River at Lamgadi, propped cantilever bridges need to be carefully designed and constructed. Errors in assumed and constructed support conditions can be detrimental to such bridges, similar to any other structure. The failure case described in this study is under self-weight only, which is relatively easier to prevent than failure due to dynamic loads and other accidental loadings. Continuous monitoring of the structure using field observations and dynamic testing during operation is essential to ensure proper operation and safety of bridges.

Acknowledgments

The authors acknowledge the support provided by Nepal Engineers' Association. Tri Ratna Bajracharya is in particular thanked for his prompt initiation in forming a field reconnaissance team and providing logistic support as mandated by Nepal Engineers' Association. Rajesh Rupakhety acknowledges support from the University of Iceland Research Fund. The opinions, findings, and conclusions expressed in this paper are those of the authors and do not necessarily represent the views of the institutions the authors are affiliated with or the institutions mentioned in this section.

Authors' contributions

Rabindra Adhikari: Conceptualization, Formal analysis, Investigation, Software, Data Curation, Writing-Original Draft. Lalit Bhatt: Investigation, Data Curation, Writing – Review & Editing. Rewati Baruwal: Investigation, Data Curation, Writing – Review & Editing. Dipendra Gautam: Conceptualization, Investigation, Validation, Data Curation, Writing-Original Draft. Rajesh Rupakhety: Validation, Resources, Writing-Review & Editing.

Funding

This research received no external funding.

Availability of data and materials

The datasets used and/or analyzed during the current study are available from the corresponding author on reasonable request.

Declarations

Competing interests

The authors declare that they have no competing interest.

Received: 3 December 2023 Accepted: 15 January 2024

Published online: 02 February 2024

References

- Adhikari R, Jha P, Bhatt L, Thapa D, Forcellini D, Gautam D (2022) Failure Investigation of under Construction Prestressed Concrete Bridge in Chitwan, Nepal. *Infrastructures* 7(2):14. <https://doi.org/10.3390/infrastructures7020014>
- Adhikari, Rabindra, Dipendra Gautam, Pratyush Jha, Bikalpa Aryal, Kamal Ghalan, Rajesh Rupakhety, You Dong, Hugo Rodrigues, and Gokarna Motra. 2019. "Bridging Multi-Hazard Vulnerability and Sustainability: Approaches and Applications to Nepali Highway Bridges." In *Resilient Structures and Infrastructure* https://doi.org/10.1007/978-981-13-7446-3_14
- Anania L, Badalà A, D'Agata G (2018) Damage and Collapse Mode of Existing Post Tensioned Precast Concrete Bridge: The Case of Petrulla Viaduct. *Eng Struct* 162:226–244. <https://doi.org/10.1016/j.engstruct.2018.02.039>
- Bazzucchi F, Restuccia L, Ferro GA (2018) Considerations over the Italian Road Bridge Infrastructure Safety after the Polcevera Viaduct Collapse: Past Errors and Future Perspectives. *Frat Ed Integrata Strutt* 12(46):400–421. <https://doi.org/10.3221/IGF-ESIS.46.37>
- Brando, F., A. Iannitelli, L. Cao, E. A. Malsch, G. Panariello, J. Abruzzo, and M. J. Pinto. 2013. "Forensic Investigation Modeling (FIM) Approach: I35 West Bridge Collapse Case Study." In *Forensic Engineering 2012: Gateway to a Better Tomorrow - Proceedings of the 6th Congress on Forensic Engineering*. <https://doi.org/10.1061/9780784412640.006>
- Bureau of Indian Standard. 2007. IS 800: 2007 General Construction in Steel-Code of Practice. India
- Calvi GM, Moratti M, O'Reilly GJ, Scattarreggia N, Monteiro R, Malomo D, Calvi PM, Pinho R (2019) Once upon a Time in Italy: The Tale of the Morandi Bridge. *Struct Eng Int* 29(2):198–217. <https://doi.org/10.1080/10168664.2018.1558033>
- Calvi, G. M., M. Moratti, N. Scattarreggia, V. Özşarac, P. M. Calvi, and R. Pinho. 2021. "Numerical Investigations on the Collapse of the Morandi Bridge." In *Developments in International Bridge Engineering: Springer Tracts on Transportation and Traffic*, edited by P. Gulkan, A. Caner, and N. Memisoglu Apaydin. 17. Springer. https://doi.org/10.1007/978-3-030-59169-4_1
- Cao Ran, El-Tawil Sherif, Agrawal Anil Kumar (2020) Miami Pedestrian Bridge Collapse: Computational Forensic Analysis. *J Bridge Eng* 25(1):04019134. [https://doi.org/10.1061/\(asce\)be.1943-5592.0001532](https://doi.org/10.1061/(asce)be.1943-5592.0001532)
- Computers and Structures Inc, CSI. 2018. "SAP2000." California
- Gautam D, Rupakhety R (2021) Empirical Seismic Vulnerability Analysis of Infrastructure Systems in Nepal. *Bull Earthq Eng* 19:6113–6127. <https://doi.org/10.1007/s10518-021-01219-5>
- Gautam D, Rupakhety R, Adhikari R (2019) Empirical Fragility Functions for Nepali Highway Bridges Affected by the 2015 Gorkha Earthquake. *Soil Dyn Earthq Eng* 126:105778. <https://doi.org/10.1016/j.soildyn.2019.105778>
- Gautam D, Adhikari R, Gautam S, Pandey VP, Thapa BR, Lamichhane S, Talchabhadel R et al (2023) Unzipping Flood Vulnerability and Functionality Loss: Tale of Struggle for Existence of Riparian Buildings. *Nat Hazards* 119:989–1009. <https://doi.org/10.1007/s11069-022-05433-5>
- Gautam D (2017) On Seismic Vulnerability of Highway Bridges in Nepal: 1988 Udaypur Earthquake (MW6.8) Revisited. *Soil Dyn Earthq Eng* 99:168–171. <https://doi.org/10.1016/j.soildyn.2017.05.014>
- Nuti C, Briseghella B, Chen A, Lavorato D, Iori T, Vanzi I (2020) Relevant Outcomes from the History of Polcevera Viaduct in Genova, from Design to Nowadays Failure. *J Civ Struct Health Monit* 10:87–107. <https://doi.org/10.1007/s13349-019-00371-6>
- Sakellariadis L, Anastasopoulos I, Gazetas G (2020) Fukae Bridge Collapse (Kobe 1995) Revisited: New Insights. *Soils Found* 60(6):1450–1467. <https://doi.org/10.1016/j.sandf.2020.09.005>
- Salem HM, Helmy HM (2014) Numerical Investigation of Collapse of the Minnesota I-35W Bridge. *Eng Struct* 59:635–645. <https://doi.org/10.1016/j.engstruct.2013.11.022>
- Scattarreggia N, Salomone R, Moratti M, Malomo D, Pinho R, Calvi GM (2022) Collapse Analysis of the Multi-Span Reinforced Concrete Arch Bridge of Capriogliola, Italy. *Eng Struct* 251:113375. <https://doi.org/10.1016/j.engstruct.2021.113375>
- Scattarreggia N, Galik W, Calvi PM, Moratti M, Orgnoni A, Pinho Rui (2022) Analytical and Numerical Analysis of the Torsional Response of the Multi-Cell Deck of a Collapsed Cable-Stayed Bridge. *Eng Struct* 265:114412. <https://doi.org/10.1016/j.engstruct.2022.114412>
- Schaap HS, Caner A (2022) Bridge Collapses in Turkey: Causes and Remedies. *Struct Infrastruct Eng* 18(5):694–709. <https://doi.org/10.1080/15732479.2020.1867198>
- Shinozuka M, Feng MQ, Lee J, Naganuma T (2002) Statistical Analysis of Fragility Curves. *J Eng Mech* 26(12). [https://doi.org/10.1061/\(asce\)0733-9399\(2000\)126:12\(1224\)](https://doi.org/10.1061/(asce)0733-9399(2000)126:12(1224))
- Sun, Zong-guang, Zhan-qi Sun, and Xiao-fei Li. 2007. "Analysis of Lateral Slippage Mechanism and Behavior for Curved Continuous Bridge." *J Highw Transp Res Dev (English Edition)* 2 (1). <https://doi.org/10.1061/jhtrcq.0000168>
- Vatansever C, Yazıcı G, Seçkin E, Alçiçek HE (2020) Failure of the Maintenance Gantry of a Metro Crossing Bridge. *Eng Fai Anal* 110:104436. <https://doi.org/10.1016/j.engfailanal.2020.104436>

Publisher's Note

Springer Nature remains neutral with regard to jurisdictional claims in published maps and institutional affiliations.